Clay mineral evolution along a soil chronosequence in an Alpine proglacial area

Mavris, C ; Plötze, M ; Mirabella, A ; Giaccai, D ; Valboa, G ; Egli, M

Abstract: As a consequence of global warming, additional areas will become ice-free and subject to weathering and soil formation. The most evident soil changes in the Alps will occur in proglacial areas where young soils will continuously develop due to glacier retreat. Little is known about the initial stages of weathering and soil formation, i.e. during the first decades of soil genesis. In this study, we investigated clay minerals formation during a time span 0–150 years in the proglacial area of Morteratsch (Swiss Alps). The soils developed on granitic till and were Lithic Leptosols. Mineralogical measurements of the clay (< 2 m) and fine silt fraction (2–32 m) were carried out using XRD (X-ray Diffraction) and DRIFT (Diffuse Reflectance Infrared Fourier Transform). Fast formation and transformation mechanisms were measured in the clay fraction. The decreasing proportion of trioctahedral phases with time confirmed active chemical weathering. Since the start of soil formation, smectite was actively formed. Some smectite (low charge) and vermiculite (high charge) was however already present in the parent material. Main source of smectite formation was biotite, hornblende and probably plagioclase. Furthermore, irregularly and regularly interstratified clay minerals (mica–HIV or mica–vermiculite) were formed immediately after the start of moraine exposure to weathering. In addition, hydroxy-interlayered smectite (HIS) as a transitory weathering product from mica to smectite was detected. Furthermore, since the start of soil evolution, kaolinite was progressively formed. In the silt fraction, only little changes could be detected; i.e. some formation of an interstratified mica–HIV or mica–vermiculite phase. The detected clay mineral formation and transformation mechanisms within this short time span confirmed the high reactivity of freshly exposed sediments, even in a cryic environment.

DOI: https://doi.org/10.1016/j.geoderma.2011.07.010

Clay mineral evolution along a soil chronosequence in an Alpine proglacial area

Christian Mavris[1], Michael Plötze[2], Aldo Mirabella[4], Daniele Giaccai[4], Giuseppe Valboa[4], Markus Egli[1]*

[1] Department of Geography, University of Zurich, Zurich, 8057, Switzerland

[2]ETH Zurich, Institute for Geotechnical Engineering, Zurich, 8093, Switzerland

[4]Istituto Sperimentale per lo Studio e la Difesa del Suolo, Centro di ricerca per l'Agrobiologia e la Pedologia, Piazza D'Azeglio 30, 50121 Firenze, Italy

*corresponding author:

tel. +41 44 635 51 14

fax: +41 44 635 68 48

e-mail: markus.egli@geo.uzh.ch

Abstract

As a consequence of global warming, additional areas will become ice-free and subject to weathering and soil formation. The most evident soil changes in the Alps will occur in proglacial areas where young soils will continuously develop due to glacier retreat. Little is known about the initial stages of weathering and soil formation, i.e. during the first decades of soil genesis. In this study, we investigated clay minerals formation during a time span 0 – 150 years in the proglacial area of Morteratsch (Swiss Alps). The soils developed on granitic till and were Lithic Leptosols.

Mineralogical measurements of the clay (< 2 µm) and fine silt fraction (2 – 32 µm) were carried out using XRD (X-ray Diffraction) and DRIFT (Diffuse Reflectance Infrared Fourier Transform). Fast formation and transformation mechanisms were measured in the clay fraction.

The decreasing proportion of trioctahedral phases with time confirmed active chemical weathering. Since the start of soil formation, smectite was actively formed. Some smectite (low charge) and vermiculite (high charge) was however already present in the parent material. Main source of smectite formation was biotite, hornblende and probably plagioclase. Furthermore, irregularly and regularly interstratified clay minerals (mica-HIV or mica-vermiculite) were formed immediately after the start of moraine exposure to weathering. In addition, hydroxy-interlayered smectite (HIS) as a transitory weathering product from mica to smectite was detected. Furthermore, since the start of soil evolution, kaolinite was progressively formed. In the silt fraction, only little changes could be detected; i.e. some formation of an interstratified mica-HIV or mica-vermiculite phase.

The detected clay mineral formation and transformation mechanisms within this short time span confirmed the high reactivity of freshly exposed sediments, even in a cryic environment.

Keywords: proglacial area, smectite, mica, kaolinite, clay minerals, soil chronosequence, Alps

Introduction

Glaciers and periods of glaciation may have a significant impact on global weathering, changing the interplay between physical and chemical weathering processes, by putting large volumes of dilute meltwaters and fine-grained sediment in contact with each other (Arn et al., 2003; Föllmi et al., 2009a,b). Due to climate warming, additional areas will become ice-free and subject to weathering and soil formation. Proglacial environments are important for the understanding of global CO_2 cycling on glacial/interglacial timescales as they made up a significant amount of the global land surface during the Quaternary due to the advance and retreat of glaciers and ice sheets (Gibbs and Kump, 1994). As stated in several previous publications (see Hosein et al.,

2004; Föllmi et al., 2009a,b; Dümig et al., 2011), the proglacial area is a potential zone of high geochemical reactivity with respect to weathering processes or organic matter accumulation. This issue is also shown by chronosequence studies. The derivation of soil chronosequence curves for main chemical elements in Alpine climates gave weathering rates (loss of mass per unit area) as a function of time. Weathering rates of young soils (age < 1000 years) on silicatic parent material seem to be two to three orders of magnitude higher than in old soils (c. 12000 years; Egli et al., 2001a). The most weathered soils in Alpine environments as well as subarctic environments are usually podzols (e.g. Gustafsson et al., 1995; Olsson and Melkerud, 2000). Also the rate of organic matter accumulation is at the beginning of soil formation much higher than in old and weathered soils (Jenny, 1980; Conen et al., 2007; Egli et al., 2010).

There is, however, not an equivocal agreement about the velocity of reaction in proglacial areas. Anderson et al. (2000) concluded from their measurements that silicate weathering is not enhanced in proglacial areas. According to them, silicate weathering reactions may be important only after vegetation cover is established. In contrast, Wadham et al. (2001), Hosein et al. (2004) and Egli et al. (2003) suggested that glacially derived material is subjected to enhanced chemical weathering (due to the dissolution of the most reactive phases such as sulphide oxidation and carbonate dissolution), starting immediately after deposition in the pro-glacial zone and subsequently continuing for thousands of years after glacier retreat. Föllmi et al. (2009a,b) measured higher biotite weathering rates in young soils (< 100 years) of a proglacial area than in old soils (11000 years).

Furthermore, two different kinds of soil production functions are discussed in literature (Humphreys and Wilkinson, 2007). Soil evolution and, consequently, weathering can be modelled using a humped or an exponential function. With a humped function, soil production and weathering is maximised at a certain soil depth or time (Gilbert, 1877; Cox, 1980; Anderson, 2002). In contrast to this approach, models using an exponential function are often applied (e.g. Heimsath et al., 1997; Egli et al., 2001a; Wilkinson et al., 2005; Humphreys and Wilkinson,

2007). According to these studies, production and weathering exponentially decreases with time. A challenge is now to test the applicability of the existing two soil production functions and as yet unknown forms to different kinds of situations.

A main gap in knowledge exists about the velocity of (clay) mineral transformations or formations in soils or material starting to be a soil in high alpine and arctic climate zones. According to Egli et al. (2003), Arn et al. (2003), Hosein et al. (2004) or Föllmi et al. (2009a), highest formation rates of clay minerals (especially smectite) or transformation rates of primary sheet silicates should be greatest at the very beginning of soil formation. There exist, however, almost no measurements for this stage of weathering or soil formation (with ages of 0 - 150 yrs) and especially related to clay mineralogical formations and transformations. The main goals of this study were consequently: i) can we detect changes in the clay mineralogy already after 150 years of soil formation in a cryic environment? ii) and if yes, can changes be attributed to specific formation and transformation processes? Consequently, we focused on the identification of clay mineral formation and transformation reaction mechanisms in a proglacial area having very young soils. Although mineral transformation reactions are often reported to be slow and almost undetectable in alpine and young areas, we hypothesised that also within a very short period of weathering changes in the clay mineralogy could be detected and assigned to transformation mechanisms. Based on this hypothesis, we want to demonstrate that alpine and cryic environments are highly reactive.

Study area

The proglacia area of Morteratsch is located in Upper Engadine, SE Switzerland (Fig. 1). The valley runs in N-S direction and the current length of the exposed area is approx. 3 km. The glacier is continuously retreating without re-advancements since the 1850s (end of the Little Ice Age; Burga, 1999) (Table 1). The moraine deposited in that period constitutes the outer border of

the investigated area. The altitude of the investigated proglacial valley ranges from 1900 m asl to approx 2150 m asl, with no abrupt stacks and slopes along its main axis. The glacial till consists of granite and gneissic material (Table 1). The morainic material was produced through glacial transport within a small area of relatively homogeneous parent material.

Geologically, the proglacial area of Morteratsch is set in the Lower Austroalpine Bernina Nappe, which is mainly constituted by plutonic rock types, such as granodiorites and diorites, syenites and alkali-granites. Accessory rocks such as dolomites, gabbros and serpentines are also reported, but are rare (Büchi, 1987; Büchi, 1994). These units underwent a 'Greenschists' facies metamorphic event during the High Alpine orogenesis event (Oligocene-Eocene; Trommsdorff and Dietrich, 1999). This event was the reason for a 'saussuritisation' process, which partially transformed primary rock forming plagioclases into albite, epidote, calcite and zeolites (D'Amico et al., 1998). Furthermore, Na-Ca-amphiboles formed as well (Büchi, 1994). The vegetation cover of the Morteratsch proglacial area has been studied by Burga (1999).

The first flowering plants colonising young deglaciated surfaces are scattered individuals of *Epilobium fleischeri* and *Linaria alpina* that appear after about 7 years. First plants of the community *Oxyrietum digynae* appear after c. 12 years and disappear after c. 27 years. The second most important community is the green alder community, which starts early and grows continuously in importance until it overtakes the Epilobietum fleischeri after about the 100 first years of succession (Burga et al., 2010). The establishment of *Larici-Pinetum cembrae* forests (open larch-Swiss stone pine forest) takes place after about 77 years (Burga, 1999) on sites where the soil is more intensely weathered. The following vegetation could be encountered at the individual sites: open larch-Swiss stone pine forest at the site S2 (Fig. 1; see also Table 2), green alder scrub at the sites S3, S4, S5, S8 and S9, Epilobietum fleischeri with single willow shrubs at site S6, pioneer grass communities at site S7 and S10. The soils are weakly developed and are mostly Lithic Leptosols (IUSS Working Group WRB, 2006).

Present climatic conditions for the Morteratsch site are approx. 0.5 °C mean annual temperature

and approx. 1000 – 1300 mm mean annual precipitation (EDI, 1992).

Materials and methods

Soil sampling

10 topsoil (uppermost, mineral horizon) samples were collected across the proglacial area of Morteratsch (Fig. 1). The sites were chosen from an existing soil chronosequence ranging from 0 – 150 yr old soils (Table 2). Approximately 1 – 2 kg of material was collected per sample.

Typical soil characteristics

Soil pH was measured in 0.01 M $CaCl_2$ using a soil solution ratio of 1:2.5. The particle size distribution was determined on some selected soil samples. After a pre-treatment of the samples with H_2O_2 (3%), particle size distribution of the soils was measured by a combined method consisting of sieving the coarser particles (32 – 2000 µm) and the measurement of the finer particles (< 32 µm) by means of an X-ray-sedimentometer (SediGraph 5100). The weight proportion of soil skeleton was determined by sieving the bulk soil material (2 mm sieve).

Fractionation of the clay (< 2 µm) and fine silt fraction (2-32 µm)

The clay fraction (< 2 µm) was collected from the parent material (averaged from the parent material of 6 monitored sites and one sample of freshly exposed subglacial sediment, collected at the glacier front) and 6 topsoils (that were representative for the selected chronosequence; sites S1, S3, S6, S7, S8, S10; see Table 2), i.e. the uppermost mineral horizon, and was analysed in detail. To separate the clay fraction (< 2µm), the fine earth samples (< 2 mm) were pre-treated at room temperature with diluted and Na-acetate buffered (pH 5) H_2O_2 to remove organic matter. The clay fraction was obtained by dispersion with Calgon and sedimentation in water.

Specimens were then Mg-saturated, washed free of chloride and freeze-dried.

The fine-silt fraction (< 32 μm) was obtained after the extraction of the clays by wet sieving. This fraction was then Mg saturated ($MgCl_2$ 2M), washed free of chlorides and freeze-dried.

X-ray diffraction analyses of the clay fraction

Textured specimens, prepared by sedimentation on glass slides from a water suspension, were analysed using a 3-kW Rigaku D/MAX III C diffractometer, equipped with a horizontal goniometer and a graphite monochromator, using Cu-Kα radiation. Slides were step-scanned from 2 to 15°2θ with steps of 0.02°2θ and 2 seconds counting time. The measurements were carried out after the following treatments were performed: Mg-saturation, ethylene glycol solvation and K saturation, followed by heating for 2 hours at 335°C and 550°C.

In a further step, the Na-citrate treatment (modified after Tamura, 1958) was performed to extract hydroxy-Al (or Fe) polymers from the interlayers of 2:1 clay minerals to check whether HIS (hydroxy-interlayered smectites) or HIV (hydroxy-interlayered vermiculites) were present. The citrate treatment enabled us to infer the presence of low-charged 2:1 clay minerals, whose expansion was hindered in the untreated state by interlayered polymers. After this treatment, HIS behaves like a 'normal' smectite when EG solvated. The Tamura procedure (Tamura, 1958) was applied in a modified form in which a contact time of 24 h without extractant removal was obtained by heating the samples in an autoclave at 135°C. After the Na-citrate procedure, the samples were Mg-saturated, ethylene glycol solvated and K saturated, followed by heating for 2 hours at 335°C and 550°C. XRD patterns of the treated samples were then compared with those of the corresponding untreated samples.

The *d*(060) region of sheet silicates was studied on random mounts. The 58 to 64°2θ range was step-scanned with steps of 0.02°2θ at 10 seconds counting time using a Bragg-Brentano diffractometer (BRUKER AXS D8, CuKα with automatic θ compensating slits and graphite monochromator). For a better distinction of trioctahedral phases, the peak position at 0.182 nm,

typical for quartz, was then compared to the one at 0.1542 nm, whose intensity is the same (Moore and Reynolds, 1997). Layer-charge estimation of smectites was performed using the long-chain alkylammonium ion C18 (and C12) according to the method proposed by Olis et al. (1990).

For the monolayer to bilayer transition, the following equation was used:

C18: $d(001) = 8.21 + 34.22\xi$

with ξ= mean layer-charge and d-values given in Å.

For the bilayer to pseudotrimolecular layer transition, the equation is:

C18: $d(001) = 8.71 + 29.65\xi$

X-ray diffraction analyses of the fine-silt fraction

The fine-silt fraction (32 – 2 μm) of the parent material (t = 0 yr) and the oldest topsoil (t = 138 yr) was chosen for an overview of the occurring mineralogical transformations The XRD measurements were carried out following the same procedure as for the clay fraction (except the citrate treatment).

XRD Data evaluation

Digitised X-ray data were smoothed and corrected for Lorentz and polarisation factors (Moore and Reynolds, 1997). Diffraction patterns were smoothed by a Fourier transform function and fitted by the Origin™ PFM program using the Pearson VII algorithm. Background values were calculated by means of a non-linear function (polynomial 2nd order function; Lanson, 1997).

The semi-quantitative estimation of phyllosilicate concentration was performed by the combination of the individual peak areas of the ethylene glycol solvated, the Mg-saturated, the K-saturated and the heated (335 °C and 550 °C) samples. On the basis of the obtained integrals, an estimate of clay minerals composition was performed. The sum of the areas between 2 and 15°2θ, which were attributed to HIV (hydroxy interlayered vermiculites), smectite, vermiculite,

mica, chlorite and kaolinite, were normalised to 100%. The relative change of the areas, with respect to the treatments, enabled the above mineral phases to be distinguished. For the Mg-saturated and for the ethylene glycol solvation treatment, the area of the following peaks (d-spacings) had to be corrected by a weighting factor F: 1.6 nm with F = 0.453, 1.4 nm with F = 0.478, and 0.71 nm with F = 0.16 (Schwertmann and Niederbudde, 1993; Gjems, 1967; Laves and Jahn, 1972; Niederbudde and Kussmaul, 1978). This procedure allowed the estimation of the relative concentrations of sheet-silicates in the clay fraction. Although the (semi-)quantification of clay minerals in soils is bedevilled by manifold problems (Kahle et al., 2002), the applied and standardised (sample preparation, treatments, measurement and calculation) procedure enabled the assessment of the variability of clay mineral assemblage amongst the sites.

The same semi-quantitative approach was already successfully used in other mineralogical studies of Alpine soils (e.g., Egli et al., 2001b; 2003; Favilli et al., 2009).

Diffused Reflectance Infrared Fourier Transform (DRIFT)

When chlorite was found using XRD, the presence of kaolinite was checked with FT-IR (Brooker Optics, Tensor 27) analysis (OH-stretching bands near 3690 cm^{-1}). About 10 mg of clay material and 350 mg of KBr were homogenised in a mill using a fine ball-mill (Zr) for 45 s (frequency 25.0). Prior to measurement, the samples were dried in the oven at 70°C. Spectra were recorded from 4000 to 250 cm^{-1}. The evaluation of FT-IR spectra was performed using OPUS 6 software.

Results

X-ray diffraction of clay fraction

In all samples, relatively sharp and clear peaks could be identified at 1.42, 1.23, 0.99, 0.85 and

0.71 nm (Fig. 2). Small peaks were detectable at 1.64 and 0.64 nm. Mg- and K-saturation and the subsequent heating treatments allowed the identification of chlorite (1.42 nm, after heating at 550°C), some hydroxy-interlayered vermiculite (HIV) and interstratified mica-HIV having chloritic layers. According to Ezzaïm et al. (1999) and Turpault et al. (2008), the peaks persisting at 1.23 nm after heating at 550°C can be attributed to chloritic layers in the mica-HIV phase. Already in the parent material (t = 0 yr; freshly exposed sediment), a small amount of smectite could be detected (1.64 nm following ethylene glycol solvation). The peaks at 0.64 nm and 0.85 nm could be attributed to plagioclase and amphibole, respectively. Some kaolinite was also identified by the peak at 0.71 nm, as confirmed by DRIFT (Fig. 3).

In the sample having an age of 48 years, the same minerals described above were detected. Nonetheless, some smaller changes in the clay mineral assemblage could be measured already after 48 yr of weathering (Fig. 4). Smectite (1.61 nm) became more significant than in the parent material. Furthermore, the amount of interstratified mica-HIV increased. Also mica started to transform – shown by the broader peak at 0.99 nm (with a minor peak at 1.03 nm). In addition, some pedogenic kaolinite (with a *d*(001) at 0.72 nm; see also Caner et al., 2010) seemed to form. This is, however, not fully clear as the *d*(002) reflection of chlorite could interfere at this position.

The clay mineralogy after 58 yr of weathering was similar to that of the previously-described soil, except for the slightly broader peak at 1.00 nm. This shows that weathering of mica progressively continues (with the formation of some mixed-layered minerals). An expandable mineral with a *d*-spacing of 1.57 nm in the EG-solvated sample indicated some interstratification of smectite with a high-charged (smectite-vermiculite or smectite-mica) or even low-charged component (smectite-HIS).

Mg-saturated and EG-solvated clay samples from the soil having an age of 78 yr exhibited XRD patterns with peaks centred at 2.43, 2.10, 1.67, 1.42, 1.23, 1.00, 0.85 and 0.71 nm (Fig. 4). The peaks at low angles were rather broad and weak. The basal reflections at 2.47 and 1.23 nm were

attributed to a regularly-interstratified mica-HIV (or mica-HIS) and/or mica-vermiculite (hydrobiotite). Additionally, the basal reflections at 2.10 and 1.04 nm pointed to a newly-formed, regularly-interstratified mica-HIV with a high proportion of mica. Some smectite was also present (1.67 nm) and was not interstratified anymore.

After 108 years of soil evolution, smectite was even better detectable. Also in this sample, regularly-interstratified mica-HIV (and/or mica vermiculite) having a substantial amount of HIV or vermiculite (with *d*(001) and *d*(002) basal reflections at 2.45 and 1.24 nm) and a component having less HIV or vermiculite (with *d*(001) and *d*(002) basal reflections at 2.12 and 1.08 nm) could be detected. In this older sample, the peak at 1.00 nm increased now substantially after K-saturation which is typical for the presence of vermiculite.

The clay mineral assemblage of the oldest soil (138 yr) was similar to that of the previously-described one. Smectite, regularly-interstratified mica-HIV and /or mica-vermiculite, vermiculite, kaolinite, chlorite, an interstratified mica-HIV (or mica-chlorite) having a high proportion of chloritic layers, mica, amphibole and plagioclase were measured. The proportion of smectite and weathered mica (interstratified mica-HIV or mica-vermiculite with a high proportion of mica) steadily increased. Compared to the parent material, more kaolinite could be measured (Fig. 3).

Na-citrate treatment of the clay fraction

Hydroxy interlayers hinder the collapse of expandable 2:1 phyllosilicates when K-saturated and the expansion of low-charge expandable minerals when EG-solvated (Barnhisel and Bertsch, 1989; Karathanasis, 1988). Citrate treatment was effective in removing the hydroxy interlayers from 2:1 phyllosilicates (Table 3). In all samples, a better resolved and clearer peak near 1.65 nm was now detected (Fig. 5). Consequently, all samples contained to a certain degree hydroxy-interlayered smectite (HIS). The peaks at very low angles (< 5° 2θ) and also between 1.00 and 1.40 nm did not shift after the Na-citrate treatment and EG solvation. HIS, therefore, occurs as a

peculiar phase and does not seem to be interstratified with mica.

The Na-citrate treatment clearly showed that additional smectitic phases were formed immediately after exposure to weathering. Remarkable changes occurred already between 0 and 48 yr of soil evolution. The general trend of the smectitic components showed a steady increase with time.

Trioctahedral and dioctahedral phases

The evaluation of XRD patterns in the d_{060} region of phyllosilicates (58 – 64° 2θ region) confirmed the presence of both trioctahedral and dioctahedral phases in the parent material (Fig. 6). The XRD pattern fitting enabled the separation of diagnostic peaks.

In general, trioctahedral species, represented by peaks in the range 59 – 61 °2θ, decreased from the parent material (youngest soil) to the oldest soil and, correspondingly, dioctahedral species (in the range 61 – 63 °2θ) increased with time. The peaks near 0.1550 and 0.1532 nm were attributed to trioctahedral chlorite and biotite, respectively. In the dioctahedral range, the peak at 0.1519 nm was attributed to Fe-rich dioctahedral phases (Fanning et al., 1989) and the one at 0.1495 nm to kaolinite that was already detected in the parent material. The peak near 0.1506 nm represents dioctahedral phases.

After 78 yr, the trioctahedral range already showed a smaller area (Fig. 6). The peak assigned to biotite (0.1536 nm) was smaller than in the parent material. A similar trend was measured for chlorite (0.1547 nm). Although not steadily, the contribution of the peak near 0.1495 nm (kaolinite) seemed to increase with time.

The oldest topsoil (t = 138 yr) was characterised by a further decrease of the trioctahedral species (Fig. 6). In contrast to that, the dioctahedral range showed a relative increase.

DRIFT and structural features

FT-IR spectra (OH-bending regions; 600 – 900 cm^{-1}) of the clay fraction of the parent material (t

= 0 yr) and oldest topsoil (t = 138 yr) are given in Figure 7. Generally, the bands associated with hydroxyl groups can be discriminated from each other, and band assignment is straightforward. Furthermore, this region is not affected by the presence of residual water molecules (Vantelon et al., 2001). The peak at 652 cm^{-1} was quite pronounced in both soils (parent material and oldest soils). This band is usually attributed to octahedral Fe and Mg in 2:1 sheet silicates (Wilson, 1994). The weak peak at 681 cm^{-1} is attributed to Fe in dioctahedral smectite (Bishop et al., 2002). Near 694 cm^{-1}, the presence of dioctahedral smectite (Van der Marel and Beutelspacher, 1976; Madejova, 2001) is confirmed already for the sample with t = 0 yr as dioctahedral smectite usually shows values close to c. 700 cm^{-1} (Wilson, 1994). The peak at 748 cm^{-1} was attributed to vermiculite (Wilson, 1994) and was detected in both samples.

The band at 787 cm^{-1}, attributed to δFeMgOH (Vantelon et al., 2001), is less distinct in the older (and more weathered) sample (138 yr). The quartz doublet was discernible as well (780 and 800 cm^{-1}; Farmer, 1974). The band at 829 cm^{-1} was assigned to δAlMgOH (Farmer, 1974). At 845 cm^{-1} a weak band attributed to calcite could be observed in the parent material. This peak was not detectable in the oldest topsoil.

Weak Si-O stretching bands, typical for trioctahedral sheet silicates, were detected at 1020 cm^{-1} and were less expressed in the 138 yr old sample (Fig. 7b; Farmer, 1974; Van der Marel and Beutelspacher, 1976; Madejova, 2001). Similarly, a weak Si-O band at circa 1030 cm^{-1} was found and attributed to newly-forming dioctahedral phases (Fig. 7b; Van der Marel and Beutelspacher, 1976; Madejova, 2001).

In the OH-stretching region, additional evidences of mineralogical transformations were detected (Fig. 3). A weak band observed at circa 3618 cm^{-1} in the oldest topsoil was related to Al in dioctahedral structures, probably smectite (Farmer, 1974; Van der Marel and Beutelspacher, 1976; Madejova, 2001). Of great interest was the peak near 3694 cm^{-1} that could be assigned to kaolinite. This vibration became more relevant in the older sample (138 yr) and is a clear sign of pedogenic kaolinite formation (Wilson, 1994).

Mean layer-charge estimation

In general, the C18 treatment showed well-developed low charged phyllosilicates with a mean layer-charge value per half unit cell (ξ) ranging from 0.27 to 0.40 in the surface horizons of the investigated soils (Fig. 8).

Low-charged phyllosilicates (with $\xi = 0.28$ per half unit cell) were detected in the parent material (t = 0 yr) and across the selected chronosequence (Fig. 8). High-charged phyllosilicates ($\xi > 0.75$) were also measured. They were partially attributed to geologically inherited smectite and vermiculite (Arocena et al., 1994), respectively. The attribution of the source parent mineral can be performed after a peak splitting procedure. The peak representing low charges ($\xi < 0.6$) could be separated into several smaller peaks. In addition to the very low charge near 0.28, charges in the range of $\xi = 0.34$-0.40 could be detected.

Silt fraction

The XRD pattern of the fine silt fraction did not reveal major transformation reactions. The peak at 0.99 nm (Fig. 9) shows some weak reflections near 1.02 nm in the oldest soil. This is related to the initial formation of an interstratification within mica. The basal reflection at 1.40 nm seemed to be slightly lower in the oldest sample. This decrease is hypothesised to be due to a weak weathering of chlorite. All other detectable phyllosilicates seemed to be unaffected by the weathering process within the investigated time range.

Discussion

Chemical weathering led already within 138 years to traceable formations and transformations of clay-sized phyllosilicates in the investigated proglacial area. An undisturbed and relatively fast soil evolution was measured. A very small amount of smectite was detected already in the parent

material. This presence might be due to hydrothermal formation or rock-water interactions that occurred below the glacier (Egli et a., 2001b). Its relative proportion in the soil clay fraction increased over time. Smectitic products could be the result of chlorite, mica and hornblende weathering, or the combination of both (Mirabella and Egli, 2003). Smectite can be taken as a kind of 'tracer-mineral' for weathering intensity in Alpine soils. Egli et al. (2001b, 2003) demonstrated for Swiss alpine regions that smectite and regularly interstratified mica/smectite are an end products of chemical weathering of chlorite and mica in strongly acidified soil horizons.

Based on the area proportion and mineral intensity factors for individual minerals (Kahle et al., 2002; Egli et al., 2003), an approximate, relative quantification of the phyllosilicate distribution in the clay fraction was made possible. With time, smectite increased (Fig. 10). Furthermore, the relative concentrations of smectite and vermiculite were negatively correlated to the amount of biotite (Fig. 11). Smectites developed from trioctahedral mica which weathered in a first step to regularly or irregularly interstratified 2:1 clay minerals (hydrobiotite or HIV-mica). Hot citrate treatment allowed the detection of hydroxy-interlayered low-charge expandable minerals (HIS). HIS was mostly a transitory product in the weathering chain of chlorite or mica to smectite transformation (Fig. 8). HIS did not seem to be intercalated with other mineral phases.

Within the investigated chronosequence, a progressive transformation of trioctahedral phases to dioctahedral was discernible in the topsoil. The decrease of trioctahedral phases (mica and chlorite) is therefore related to the increase of dioctahedral phases such as smectite, vermiculite or even kaolinite. Progressive transformation of clay mineral structures led to a decrease of layer charge caused by the substitution of Al^{3+} and Fe^{3+} for Mg^{2+} in the octahedral sheet (Fig. 6; Mirabella and Egli, 2003). The pedogenetic smectites from the surface horizons generally included various interlayer charges that are in agreement with results of Gillot et al. (2001). The heterogeneity of smectites is related to the nature of their precursors. In most cases, the higher the weathering state of the investigated soils, the lower was the layer charge of smectite.

Noteworthy is the behaviour of kaolinite. In the dioctahedral range, the diagnostic peak was already detectable in the parent material. The specific peak area increased with the duration of pedogenesis. This finding is supported by the FT-IR measurements where an increase of the bands typical for kaolinite could be observed. Consequently, active kaolinite formation is already possible within the first decades of pedogenesis.

Minor changes in the layer charge distribution could be also measured with the time span of 138 years. The parent material predominately had charges near $\xi = 0.28$ and > 0.75. Low charged clay minerals are usually rather formed during soil formation and weathering. The low charged minerals detected in the parent material either to a kind of weathering that occurred before the material was exposed to atmosphere or to some hydrothermally formed phases (Egli et al., 2001b). With time, it seems that some additional phases developed. Using the layer charges, some smectite transformation mechanisms can be hypothesised (Dreher and Niederbudde, 2000). A part of the newly formed smectite seems to derive from biotite (BDS) and another part from hornblende (HDS) and plagioclase (PDS; Aoudjit et al., 1995; Bétard et al., 2009). Hornblende-derived smectite (HDS) gives rise to a rather low charge (Fig. 8). Comparatively higher charges (i.e. $\xi > 0.4$ per $O_{10}(OH)_2$)) are typical for a biotite-derived smectite (BDS; Egli et al., 2003). Soils with highly charged smectites (i.e. $\xi \geq 0.4$), the charge of which is located in the tetrahedrons closely to 100%, have a very high K selectivity (Dreher and Niederbudde, 2000). According to Bétard et al. (2009), weathering of plagioclase produces directly illite and high-charge smectite ('plagioclase-derived smectite' PDS; Fig. 8). Some of the detected smectite in the proglacial area probably is a direct transformation product of plagioclase.

After 48 yr, layer charges near $\xi = 0.39$ and $\xi = 0.63$ were detected and attributed to newly-formed phases due to weathering (Arocena et al., 1994). The layer charge $\xi = 0.39$ is a typical value for a pedogenic HDS, while $\xi = 0.63$ rather corresponds to a BDV (biotite-derived vermiculite) or probably to a BDS (Dreher and Niederbudde, 2000). This phenomenon was observed in all investigated topsoils, where newly-formed phases were detected. In general,

geologically inherited smectite had a charge between ξ = 0.27 and 0.28 and biotite (or vermiculite) always $\xi > 0.75$. Pedogenic HDS usually showed a ξ of approximately 0.34, while BDV or BDS was detected with a charge of ξ = 0.63 (BDV, probably also BDS) or 0.40 (BDS). Higher values for smectite are typical for the initial stages of smectite formation in the soil and tend to decrease as a function of weathering (Mirabella and Egli, 2003).

Clay minerals in soils and weathered rocks are usually interpreted as secondary phyllosilicates derived from the transformation of primary rock-forming minerals with similar properties (e.g. mica) or as direct products of hydrothermal alteration of feldspar (i.e. sericite). Bétard et al. (2009) and also Aoudjit et al. (1995) were able to show that the neoformation of clays inside plagioclase crystals occur after their partial dissolution in the weathering zone.

Mineralogical transformations were clearly linked to the grain size and consequently to the surface area and reactivity. Investigations of the 32 – 2 μm fraction revealed only relatively small variations within a time span of 140 years. The initial formation of an interstratified mica-vermiculite (or mica-HIV) phase is evidenced by a weak broadening of the 1.00 nm peak.

Data on clay-mineral formation in Alpine soils over a very short time span are scarce. We showed that mineral formation and transformation mechanisms are fast and consequently also detectable within a time span of < 150 years. Smectite and kaolinite formation starts within the first decades. This finding is in agreement with the results of Caner et al. (2010). These authors investigated the soil evolution at the Oléron Island and evidenced a smectite formation (due to the weathering of illite) within < 188 years. Weathering reactions and smectite formation were driven by the production of complexing organic acids during the decomposition of the pine-needle litter. These induced a rapid acidification and subsequently clay-mineral transformation in the sandy, poorly buffered parent material.

The investigated sites are on relatively stable landscape surfaces where erosion is insignificant compared with the rates of weathering advance. In such landscapes, when soils are young and rich in nutrients, weathering is also controlled by biological processes. Over short timescales, the

impact of living organisms is quite apparent: rock weathering, soil formation and erosion, slope stability and river dynamics are directly influenced by biotic processes that mediate chemical reactions, dilate soil, disrupt the ground surface and add strength with a weave of roots (Dietrich and Perron, 2006). Brantley et al. (2011) hypothesise that on landscapes experiencing little erosion, biology drives weathering during initial succession, whereas weathering drives biology over the long term. This most probably applies also to the Morteratsch proglacial area and is the subject of ongoing investigations.

Conclusions

The clay mineral formation along a 0 – 150 yr high Alpine chronosequence was studied. We made the following, principle findings:

- Within a relatively short period of time (< 150 years), phyllosilicate transformations could be measured in the high Alpine proglacial area
- The mineral transformations were predominately restricted to the clay phase. Some minor transformations, i.e. the formation of a mica-HIV (or mica-vermiculite) phase having a low proportion of HIV or vermiculite, could be measured in the fine silt fraction.
- With time, smectite and mixed-layered minerals (such as mica-HIV or mica-vermiculite) formed at the expense of biotite.
- Probably different sources contributed to the formation of smectite formation (biotite and probably also hornblende and plagioclase).
- HIS was formed as a transitory product of mica transformation.
- Active formation of kaolinite starts with the first decades of weathering.
- As a consequence of these transformations, the a) layer charge distribution changed over time with the formation of some new low- and high-charged phases and b) dioctahedral species increased at the expense of trioctahedral ones.

Recently deglaciated areas and cryic environments seem to be highly reactive. Using these new results and those of Egli et al. (2003) and Mavris et al. (2010), no humped function (soil production function; according to the concept of Gilbert (1877)) of the weathering intensity could be observed. Weathering intensity was high since the very beginning of soil formation and no retarding effects could be observed in the investigated environmental settings.

Acknowledgements

This research was supported by the Swiss National Foundation (SNF), project grant n. 200021-117568. We would like to thank B. Kägi and M. Hilf for the help in the laboratory.

References

Anderson, S.P., Drever, J.I., Frost, C.D., Holden, P., 2000. Chemical weathering in the foreland of a retreating glacier. Geochimica et Cosmochimica Acta 64, 1173-1189.

Anderson, R.S., 2002. Modeling the tor-dotted crests, bedrock edges, and parabolic profiles of high alpine surfaces of the Wind River Range, Wyoming. Geomorphology 46, 35–58.

Aoudjit, H., Robert, M., Elsass, F., Curmi, P., 1995. Detailed study of smectite genesis in granite saprolites by analytical electron microscopy. Clay Minerals 30, 135-148.

Arn, K., Hosein, R., Föllmi, K.B., Steinmann, P., Aubert, D., Kramers, J., 2003. Strontium isotope systematics in two glaciated crystalline catchments: Rhone and Oberaar glaciers (Swiss Alps). Swiss Bulletin of Mineralogy and Petrology 83, 273-283.

Arocena, J. M., Pawluk, S., Dudas, M.J., 1994. Layer charge of expandable 2:1 phyllosilicates in selected parent materials of some Canadian soils. Canadian Journal of Soil Science 74, 291-299.

Barnhisel, R.I., Bertsch, P.M., 1989. Chlorite and hydroxy-interlayered vermiculite and smectite. In: Dixon, J.B., Weed, S.B. (Eds.), Minerals in Soil Environments. 2nd ed. Soil Science

Society of America, SSSA Book Series, 1, 729-788, Madison, WI, USA.

Bétard, F., Caner, L. , Gunnell, Y., Bourgeon, G., 2009. Illite neoformation in plagioclase during weathering: evidence from semi-arid Northeast Brazil. Geoderma, 152, 53-62.

Bishop, J., Madejova, J., Komadel, P., Fröschl, H., 2002. The influence of structural Fe, Al and Mg of the infrared OH bands in spectra of dioctahedral smectites. Clay Minerals 37, 607-616.

Brantley, S.L., Megonigal, J.P., Scatena, F.N., Balogh-Brunstad, Z., Barnes, R.T., Bruns, M.A., Van Cappellen, P., Dontsova, K., Hartnett, H.E., Hartshorn, A.S., Heimsath, A., Herndon, E., Jin, L., Keller, C.K., Leake, J.R., McDowell, W.H., Meinzer, F.C., Mozdzer, T.J., Petsch, S., Pett-Ridge, J., Pregitzer, K.S., Raymond, P.A., Riebe, C.S., Shumaker, K., Sutton-grier, A., Walter, R., Yoo, K., 2011. Twelve testable hypotheses on the geobiology of weathering. Geobiology, DOI: 10.1111/j.1472-4669.2010.00264.x

Büchi, H., 1987. Geologie und Petrographie der Bernina IX. Das Gebiet zwischen Pontresina und dem Morteratschgletscher. Unpubliziert Diplomarbeit Universität Zürich.

Büchi, H., 1994. Der variskische Magmatismus in der östlichen Bernina (Graubünden, Schweiz). Schweizerische Mineralogische und Petrographische Mitteilungen 74, 359-371.

Burga, C., 1999. Vegetation development on the glacier forefield Morteratsch (Switzerland). Applied Vegetation Science 2, 17-24.

Burga, C.A., Krüsi, B., Egli, M., Wernli, M., Elsener, S., Ziefle, M., Mavris, C., 2010. Plant succession and soil development on the foreland of the Morteratsch glacier (Pontresina, Switzerland): Straight forward or chaotic? Flora 205, 561-576.

Caner, L., Joussein, E., Salvador-Blanes, S., Hubert, F., Schlicht, J.F., Duigou, N., 2010. Short-time clay-mineral evolution in a soil chronosequence in Oleron Island (France). Journal of Plant Nutrition and Soil Science 173, 591-600.

Conen, F., Yakutin, M.V., Zumbrunn, T., Leifeld, J., 2007. Organic carbon and microbial biomass in two soil development chronosequences following glacial retreat, European Journal of Soil Science 58, 758-762.

Cox, N.J., 1980. On the relationship between bedrock lowering and regolith thickness. Earth Surface Processes 5, 271–274.

D'Amico, C., Innocenti, F., Sassi, F. P., 1998. Magmatismo e Metamorfismo. Ed. UTET, Torino.

Dietrich, W.E., Perron, J.T., 2006. The search for a topographic signature of life. Nature 439, 411-418.

Dreher, P., Niederbudde, E. A., 2000. Characterization of expandable layer silicates in humic-ferralic cambisols (umbrept) derived from biotite and hornblende. Journal of Plant Nutrition Soil Science 163, 447-453.

Dümig. A., Smittenberg, R., Kögel-Knabner, I., 2011. Concurrent evolution of organic and mineral components during initial soil development after retreat of the Damma glacier, Switzerland. Geoderma 163, 83-94

EDI (Eidgenössisches Departement des Innern), 1992. Hydrologischer Atlas der Schweiz (HADES). Landeshydrologie und -geologie, EDMZ, Bern.

Egli, M., Mirabella, A., Fitze, P. 2001a. Weathering and evolution of soils formed on granitic, glacial deposits: results from chronosequences of Swiss alpine environments. Catena 45, 19-47.

Egli, M., Mirabella, A., Fitze, P., 2001b. Clay mineral formation in soils of two different chronosequences in the Swiss Alps. Geoderma 104, 145-175.

Egli, M., Mirabella, A., Fitze, P., 2003. Formation rates of smectites derived from two Holocene chronosequences in the Swiss Alps. Geoderma 117, 81-98.

Egli, M., Mavris, C., Mirabella, A., Giaccai, D., Kägi, B., Haeberli, W., 2010. Soil organic matter formation along a chronosequence in the Morteratsch proglacial area (Upper Engadine, Switzerland). Catena 82, 61-69.

Ezzaïm, A., Turpault, M. –P., Ranger, J., 1999. Quantification of weathering processes in an acid brown soil developed from tuff (Beaujolais, France) Part II. Soil formation. Geoderma 87, 155-177.

Fanning, D.S., Keramidas, V.Z., El-Desoky, M.A., 1989. Micas. In: Dixon, J.B., Weed, S.B. (Eds.), Minerals in Soil Environment. 2nd Ed. Soil Science Society of America, Madison, WI, USA, pp. 551-634.

Farmer, V.C., 1974. Layer silicates. In: Farmer V.C. (ed.), Infrared Spectra of Minerals, Monograph 4, Mineralogical Society, London, pp 331-363.

Favilli, F., Egli, M., Brandova, D., Ivy-Ochs, S., Kubik, P., Cherubini, P., Mirabella, A., Sartori, G., Giaccai, D., Haeberli, W., 2009. Combined use of relative and absolute dating techniques for detecting signals of Alpine landscape evolution during the late Pleistocene and early Holocene. Geomorphology 112, 48-66.

Föllmi, K.B., Arn, K., Hosein, R., Adatte, T., Steinmann, P., 2009a. Biogeochemical weathering in sedimentary chronosequences of the Rhône and Oberaar Glaciers (Swiss Alps): rates and mechanisms of biotite weathering. Geoderma 151, 270-281.

Föllmi, K.B., Hosein, R., Arn, K., Steinmann, P., 2009b. Weathering and the mobility of phosphorus in the catchments and foefields of the Rhône and Oberaar glaciers, central Switzerland: Implications for the global phosphorus cycle on glacial-interglacial timescales. Geochimica et Cosmochimica Acta 73, 2252-2282.

Fordham, A. W., 1990. Weathering of biotite into dioctahedral clay minerals. Clay Minerals 25, 51-63.

Gibbs M. T., Kump L. R., 1994. Global chemical erosion during the last glacial maximum and the present: Sensitivity to changes in lithology and hydrology. Paleoceanography 9, 529–543.

Gilbert, G.K., 1877. Report on the Geology of the Henry Mountains. U.S. Geographical and Geological Survey of the Rocky Mountain Region, Washington, D.C.

Gillot, F., Righi, D., Räisänen, M.L., 2001. Layer-charge evaluation of expandable clays from a chronosequence of podzols in Finland using an alkylammonium method. Clay Minerals 36, 571-584.

Gjems, O., 1967. Studies on clay minerals and clay mineral formation in soil profiles in Scandinavia. Norske Skogfersøksvesen 81, 301-415.

Gustafsson, J.P., Bhhattacharya, P., Bain, D.C., Fraser, A.R., McHardy, W.J., 1995. Podzolisation mechanisms and the synthesis of imogolite in northern Scandinavia. Geoderma 66, 167-184.

Heimsath, A.M., Dietrich, W.E., Nishiizumi, K., Finkel, R.C., 1997. The soil production function and landscape equilibrium. Nature 388, 358–361.

Hosein, R., Arn, K., Steinmann, P., Adatte, T., Föllmi, K. B., 2004. Carbonate and silicate weathering in two presently glaciated, crystalline catchments in the Swiss Alps. Geochimica et Cosmochimica Acta 68, 1021-1033.

Humphreys, G.S., Wilkinson, M.T., 2007. The soil production function: A brief history and its rediscovery. Geoderma 139, 73-78.

IUSS Working Group WRB. World Reference Base for Soil Resources 2006, 2nd edition, World Soil Resources Reports No. 103, FAO (Food and Agriculture Organisation of the United Nations), Rome, 2006.

Jenny, H., 1980. The Soil Resource. Origin and Behavior. Ecological Studies 37, Springer-Verlag, New York.

Kahle, M., Kleber, M., Jahn, R., 2002. Review of XRD-based quantitative analyses of clay minerals in soils: the suitability of mineral intensity factors. Geoderma 109, 191-205.

Karathanasis, A.D., 1988. Compositional and solubility relationships between aluminum-hydroxy interlayered soil-smectites and vermiculites. Soil Science Society of America Journal 52, 1500-1508.

595 Lanson, B., 1997. Decomposition of experimental X-ray diffraction patterns (profile fitting): a
596 convenient way to study clay minerals. Clays and Clay Mineralogy 45, 2, 132-146.
597 Laves, D., Jahn, G., 1972. Zur quantitativen röntgenographischen Bodenton-Mineralanalyse.
598 Archiv für Acker-, Pflanzenbau und Bodenkunde 16, 735-739.
599 Madejova, J., Komadel, P., 2001. Baseline studies of the clay minerals society source clays:
600 Infrared methods. Clays and Clay Minerals 49, 5, 410-432.
601 Mavris, C., Egli, M., Plötze, M., Blum, J.D., Mirabella, A., Giaccai, D., Haeberli, W., 2010.
602 Initial stages of weathering and soil formation in the Morteratsch proglacial area (Upper
603 Engadine, Switzerland). Geoderma 155, 359-371
604 Mirabella, A., Egli, M., 2003. Structural transformations of clay minerals in soils of a
605 climosequence in an Italian Alpine environment. Clays and Clay Minerals 51, 3, 264-278.
606 Moore, D.M., Reynolds Jr., R.C., 1997. X-ray diffraction and the identification and analysis of
607 clay minerals. 2nd edition, Oxford University Press, New York.
608 Niederbudde, E.A., Kussmaul, H., 1978. Tonmineraleigenschaften und –Umwandlungen in
609 Parabraunerde-Profilpaaren unter Acker und Wald in Süddeutschland. Geoderma 20, 239-
610 255.
611 Olis, A. C., Malla, P. B., Douglas, L. A., 1990. The rapid estimating of the layer charges of 2:1
612 expanding clays from a single alkylammonium ion expansion. Clay Minerals 25, 39-50
613 Olsson, M.T., Melkerud P.-A., 2000. Weathering in three podzolized pedons on glacial deposits
614 in northern Sweden and central Finland. Geoderma, 94, 149-161.
615 Schwertmann, U., Niederbudde, E. A., 1993. Tonmineralbestimmung in Böden. In: Jasmund, K.,
616 Lagaly, G. (eds.), Tonminerale und Tone. Struktur, Eigenschaften, Anwendung und Einsatz in
617 Industrie und Umwelt. Steinkopff Verlag, Darmstadt, pp. 255-265.
618 Tamura, T., 1958. Identification of clay minerals from acid soils. Journal of Soil Science 9, 141-
619 147.

Trommsdorff, V., Dietrich, V., 1999. Grundzüge der Erdwissenschaften. vdf-Verlag, 6. Auflage, Zürich, Switzerland.

Turpault, M.-P., Righi, D., Utérano, C., 2008. Clay minerals: Precise markers of the spatial and temporal variability of the biogeochemical soil environment. Geoderma 147, 3-4, 108-115.

Van der Marel, H.W., Beutelspacher, H., 1976. Atlas of Infrared Spectroscopy of Clay Minerals and Their Admixtures. Elsevier Scientific Publishing Company, Amsterdam-Oxford-New York.

Vantelon, D., Pelletier, M., Michot, L.J., Barres, O., Thomas, F., 2001. Fe, Mg and Al distribution in the octahedral sheet of montmorillonites. An infrared study in the OH-bending region. Clay Minerals 36, 369-379.

Wadham, J.L., Cooper, R.J., Tranter, M., Hodgkins, R., 2001. Enhancement of glacial solute fluxes in the proglacial zone of a polythermal glacier. Journal of Glaciology 47, 378-386.

Wilkinson, M.T., Chappell, J., Humphreys, G.S., Fifield, K., Smith, B., Hesse, P.P., 2005. Soil production in heath and forest, BlueMountains, Australia: influence of lithology and palaeoclimate. Earth Surface Processes and Landforms 30, 923–934.

Wilson, M.J., 1994. Clay Mineralogy: Spectroscopic and Chemical Determinative Methods. Chapman & Hall, London.

Figure captions

Fig. 1. Location of the Morteratsch proglacial area (SE Switzerland), with isochrones (after Burga, 1999) and monitored sites.

Fig. 2. XRD patterns of the parent material of site S1 (t = 0 yr) and the oldest topsoil (t = 138 yr, S1; see also Table 2). The XRD curves were smoothed and corrected for Lorentz and polarization factors. *d*-spacings are given in nm. EG = ethylene glycol solvation, Mg = Mg-saturation, K = K-saturation and corresponding heating treatments.

Fig. 3. Comparison of FT-IR spectra of clay fraction in the OH-stretching region (range 3200-3900 cm^{-1}) between t = 0yr (thin line; parent material of site S1) and t = 138yr (thick line; topsoil of S1).

Fig. 4. XRD patterns of the EG-solvated clay fraction from the selected topsoils along the chronosequence. Given are the measured values (squares), modelled elementary curves and the modelled overall curve.

Fig. 5. XRD patterns of the Na-citrate treated and ethylene glycol (EG)-solvated soil clay fractions from selected topsoils along the chronosequence. The XRD curves were smoothed and corrected for Lorentz and polarization factors. *d*-spacings are given in nm. Given are the measured values (squares), modelled elementary curves and the modelled overall curve.

Fig. 6. XRD patterns in the d_{060} region of the soil clays from three investigated sites as a function of time. The peak range between 0.1560 and 0.1530 nm was assigned to trioctahedral and the one between

0.1530 and 0.1480 to dioctahedral phases. Given are the measured values (squares), modelled elementary curves and the modelled overall curve.

Fig. 7. Comparison of FT-IR spectra in the OH bending (A) and M-O region (B) between t = 0 yr (thin line) and t = 138 yr (thick line).

Fig. 8. XRD patterns of soil clays (< 2μm) along the chronosequence. Clays were treated with C18 (18-alkylammonium ion). The XRD-curves were corrected for Lorentz and polarization factors. *d*-spacings are given in nm. The bold numbers indicate the calculated layer charge per half unit cell. BDV = biotite derived vermiculite, HDS = hornblende derived smectite, IS = geologically inherited smectite, IV = inherited vermiculite, BDS = pedogenic biotite berived smectite, PDS = plagioclase derived smectite. Given are the measured values (squares), modelled elementary curves and the modelled overall curve.

Fig. 9. XRD patterns of EG-solvated silt fractions (32 – 2 μm) from t = 0 yr and t = 138 yr topsoil. The XRD curves were smoothed and corrected for Lorentz and polarization factors. *d* spacings are given in nm. Given are the measured values (squares), modelled elementary curves and the modelled overall curve.

Fig. 10. Smectite content in the clay fraction along the chronosequence. Statistical significance (p) is < 0.05.

Fig. 11. Correlation between the sum of smectite and vermiculite and the mica content (clay fraction). Symbols: circles for topsoils, square for parent material. Statistical significance (p) is < 0.10.

Figure 1

Click here to download high resolution image

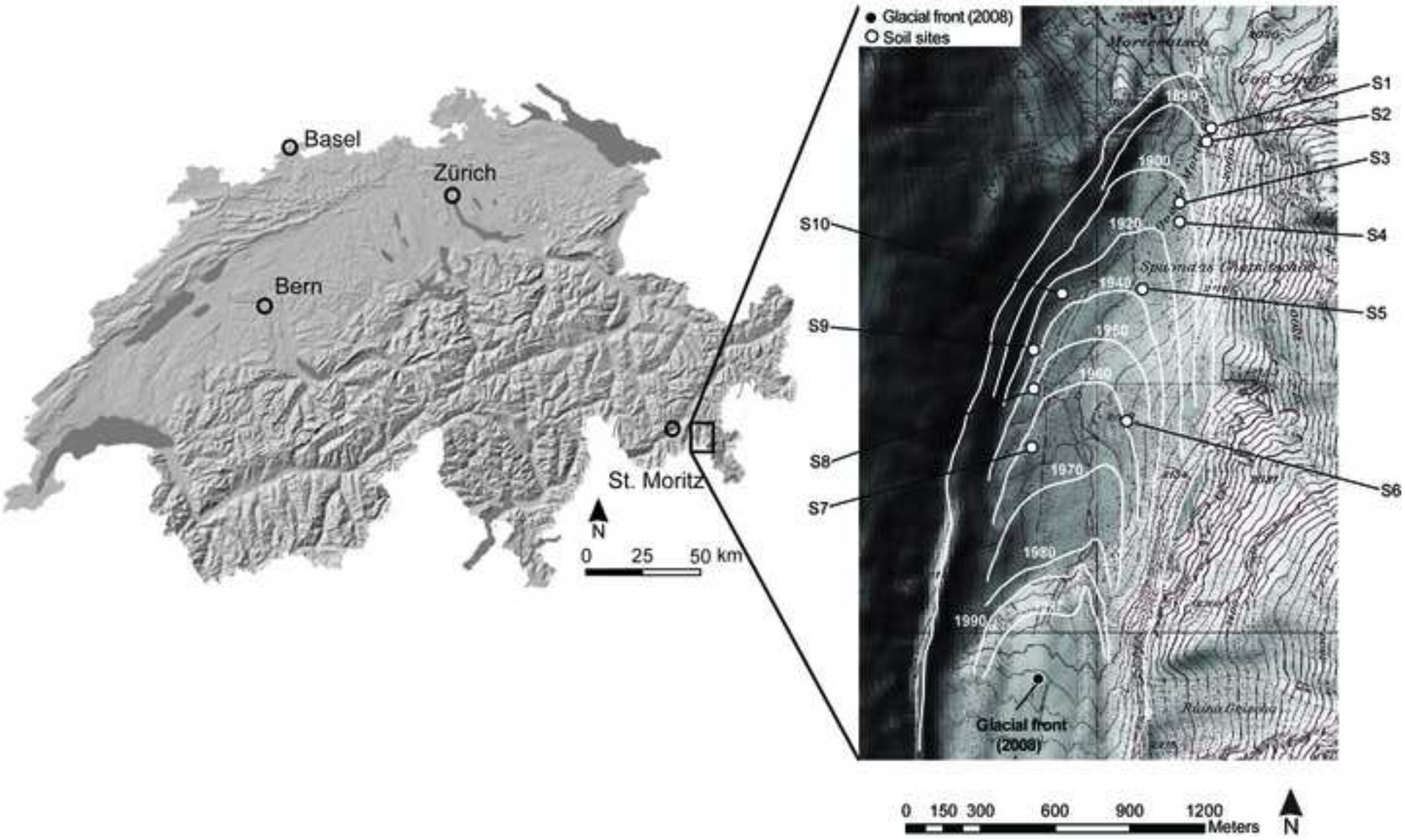

Figure 2

Click here to download high resolution image

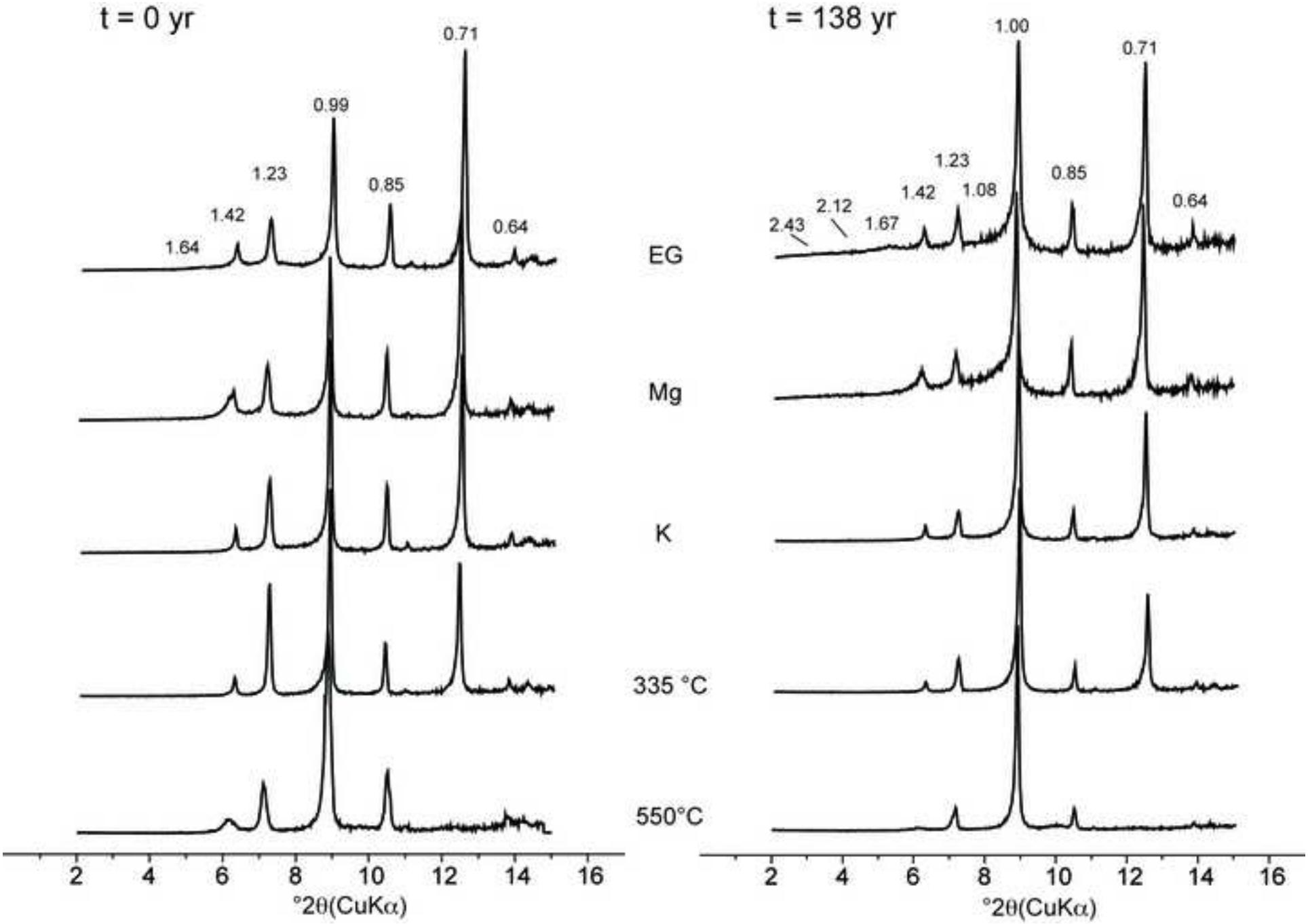

Figure 3

Click here to download high resolution image

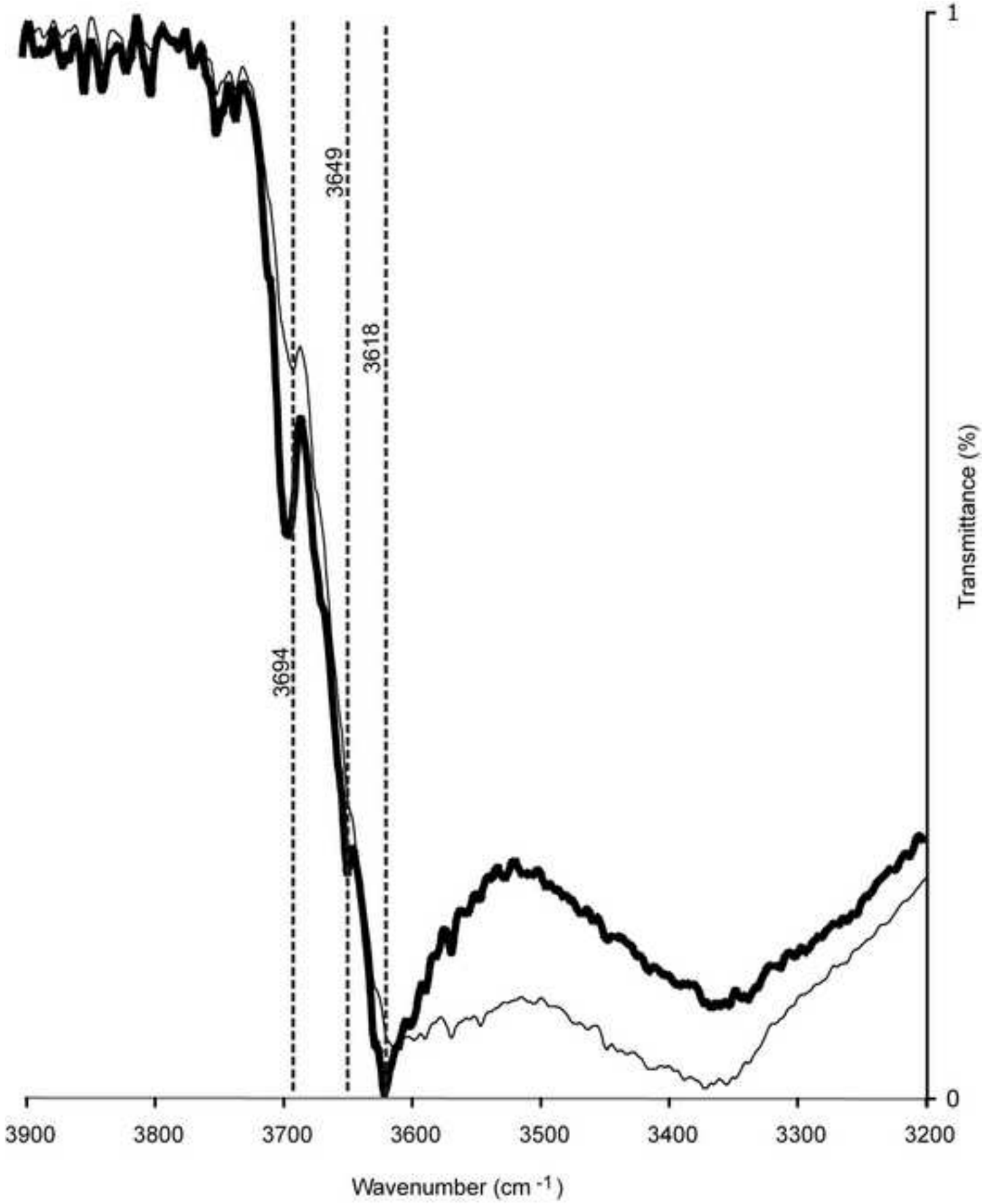

Figure 4

Click here to download high resolution image

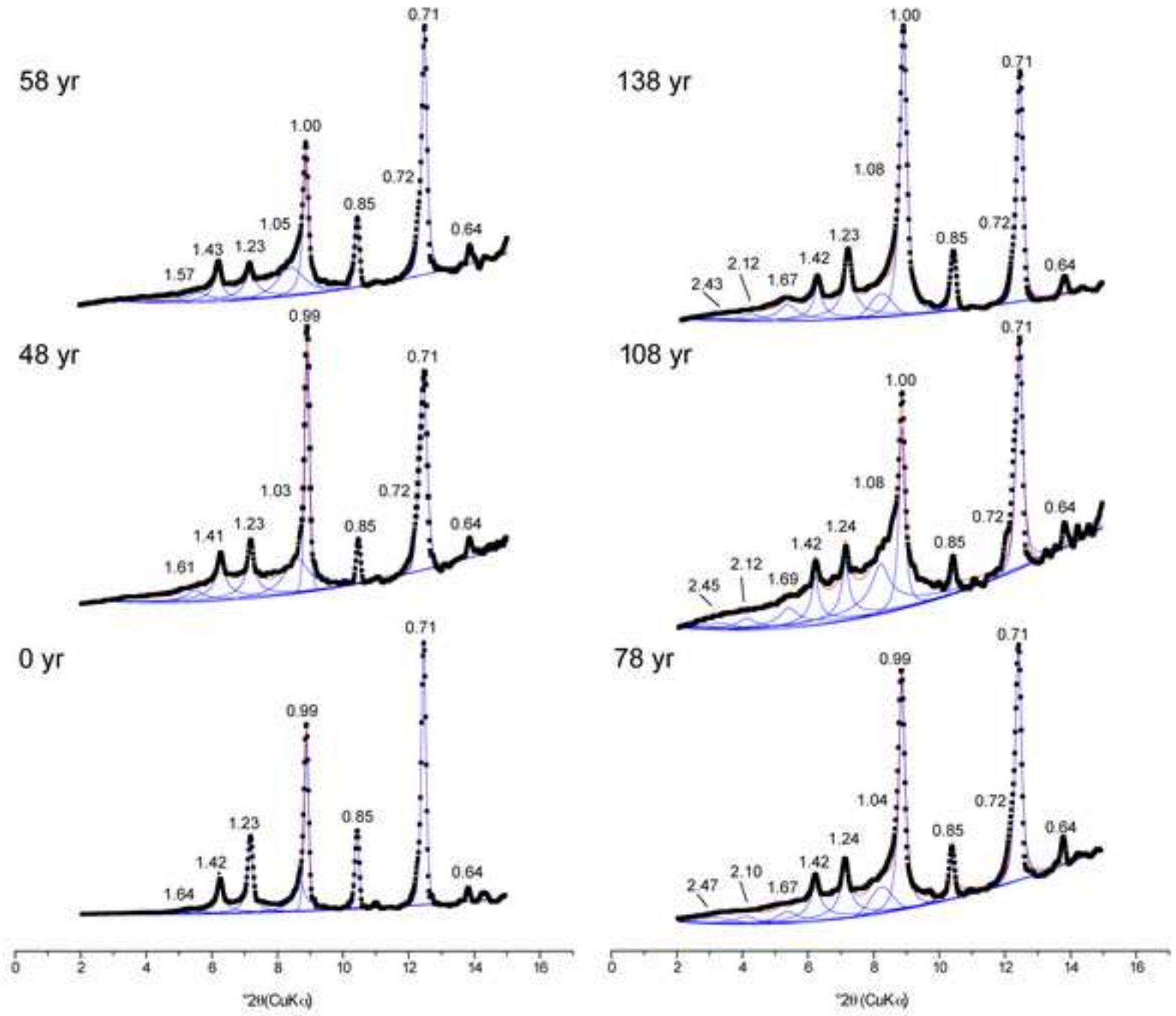

Figure 5

Click here to download high resolution image

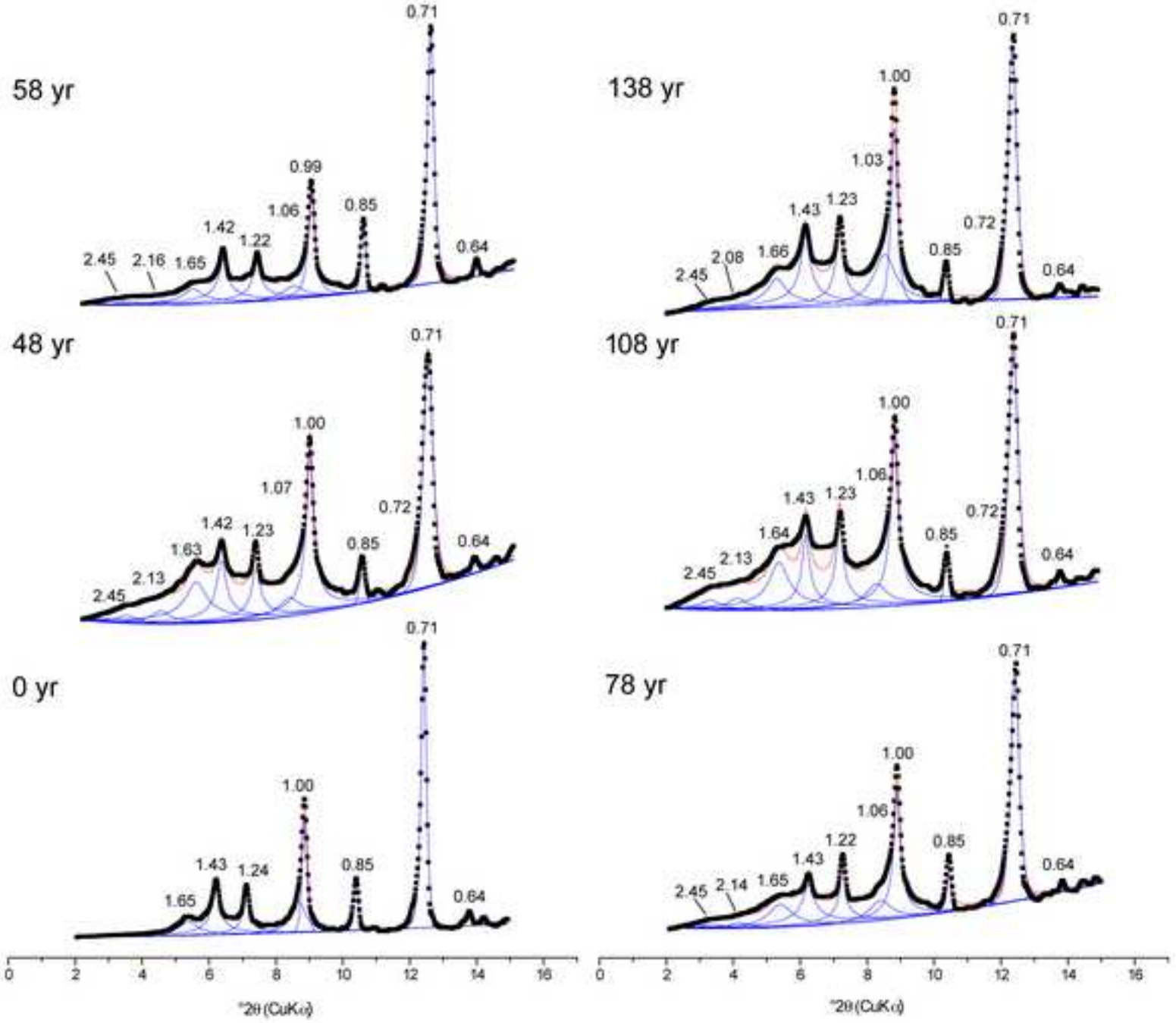

Figure 6

Click here to download high resolution image

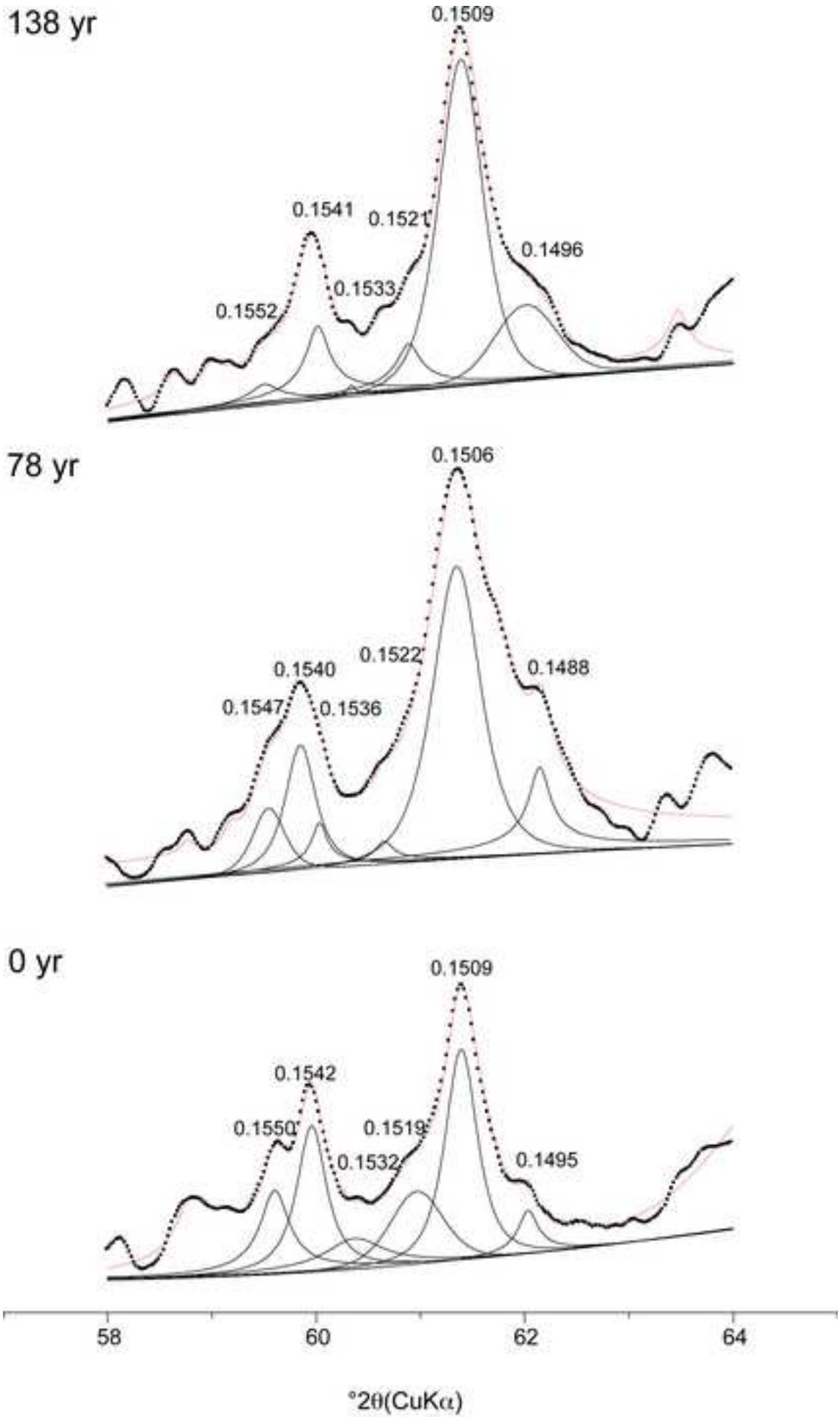

Figure 7

Click here to download high resolution image

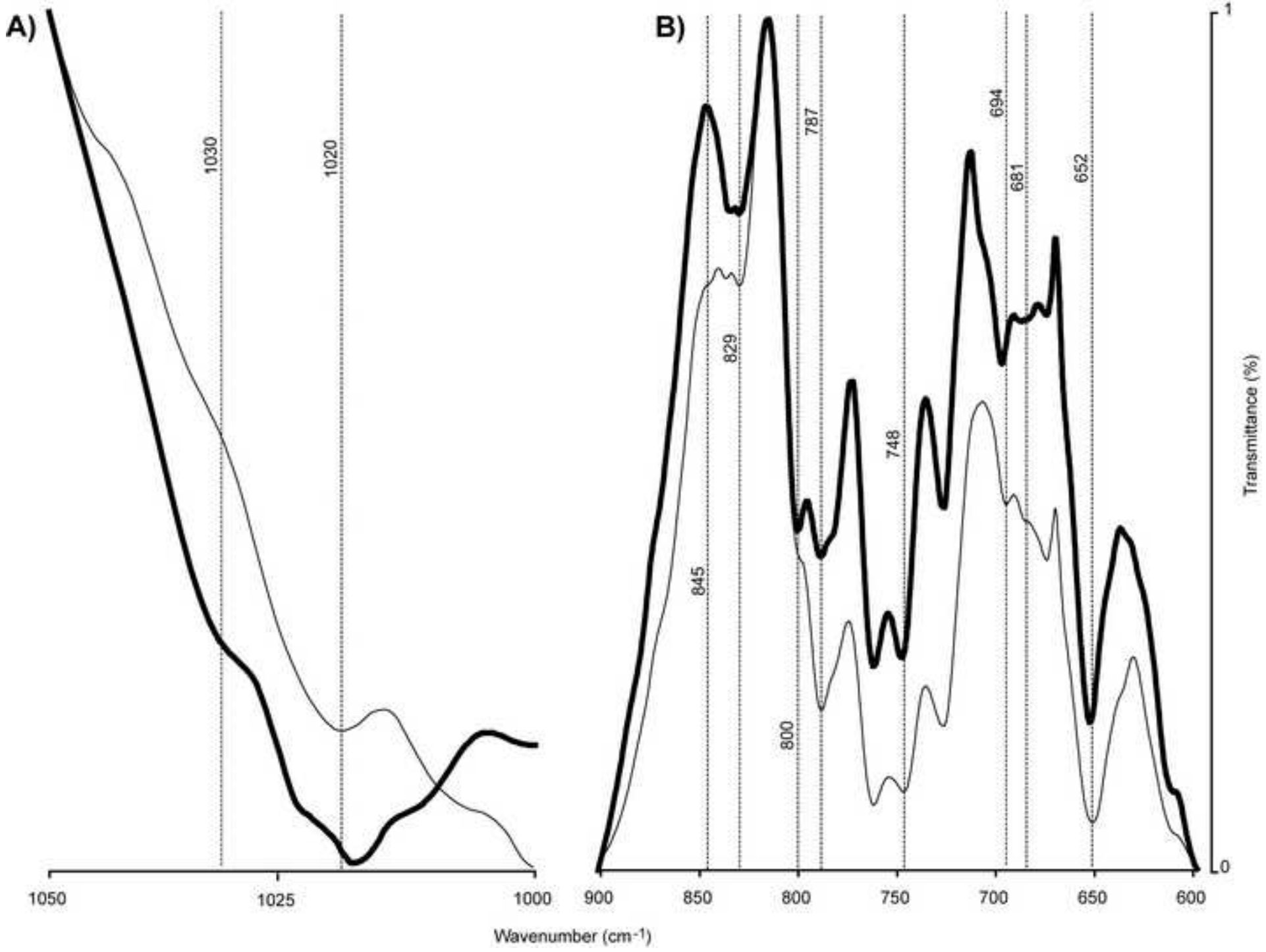

Figure 8

Click here to download high resolution image

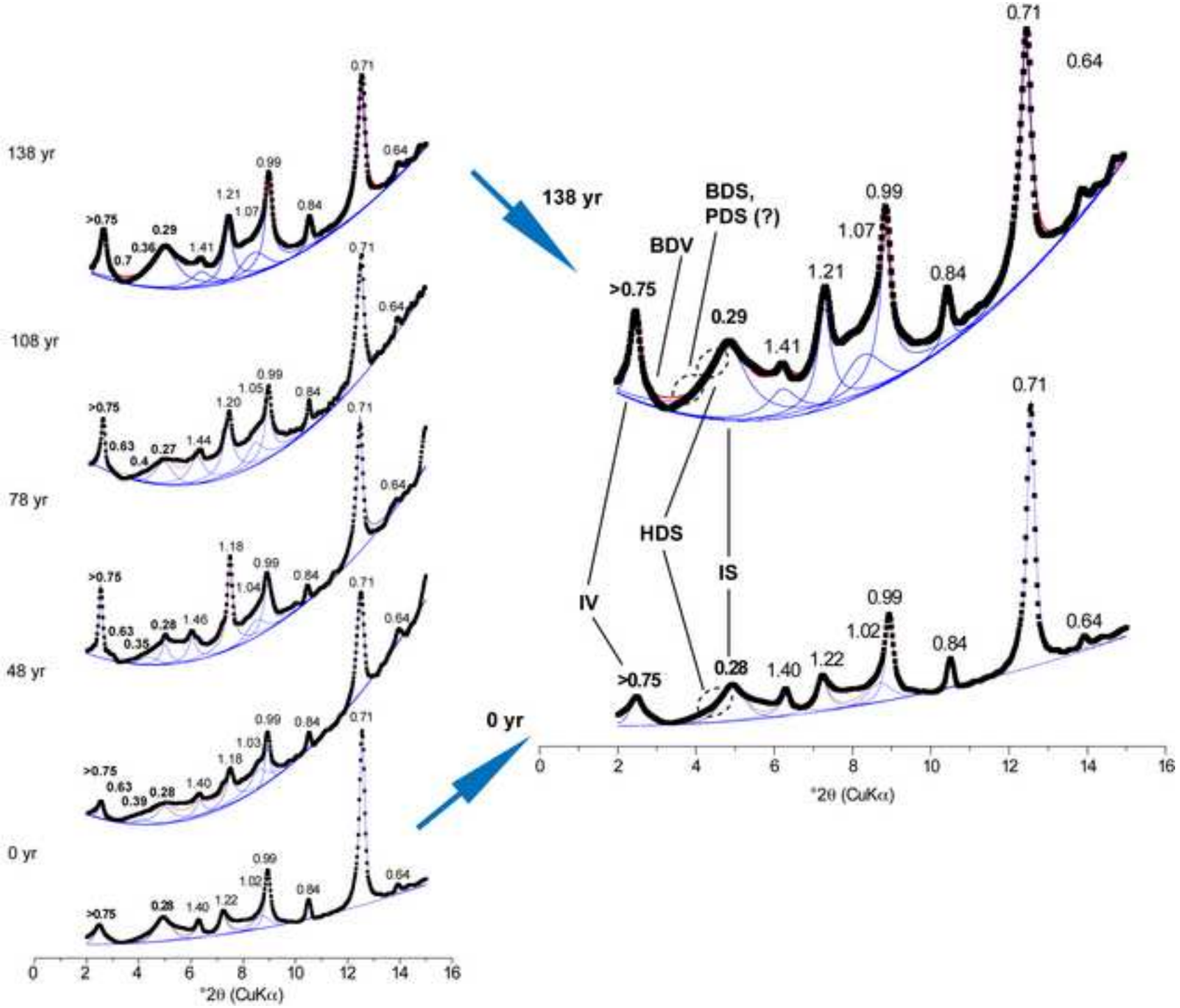

Figure 9

Click here to download high resolution image

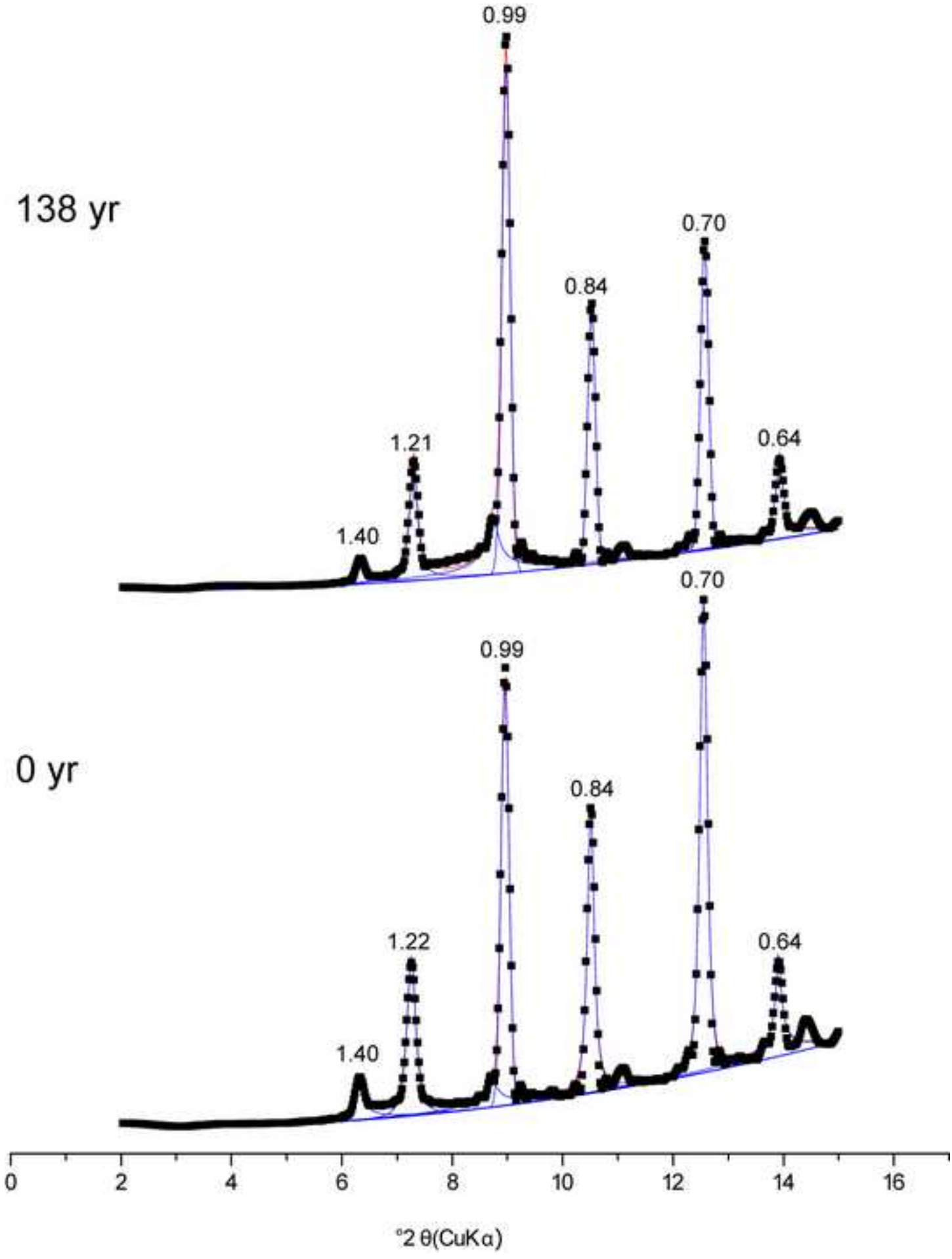

Figure 10
Click here to download high resolution image

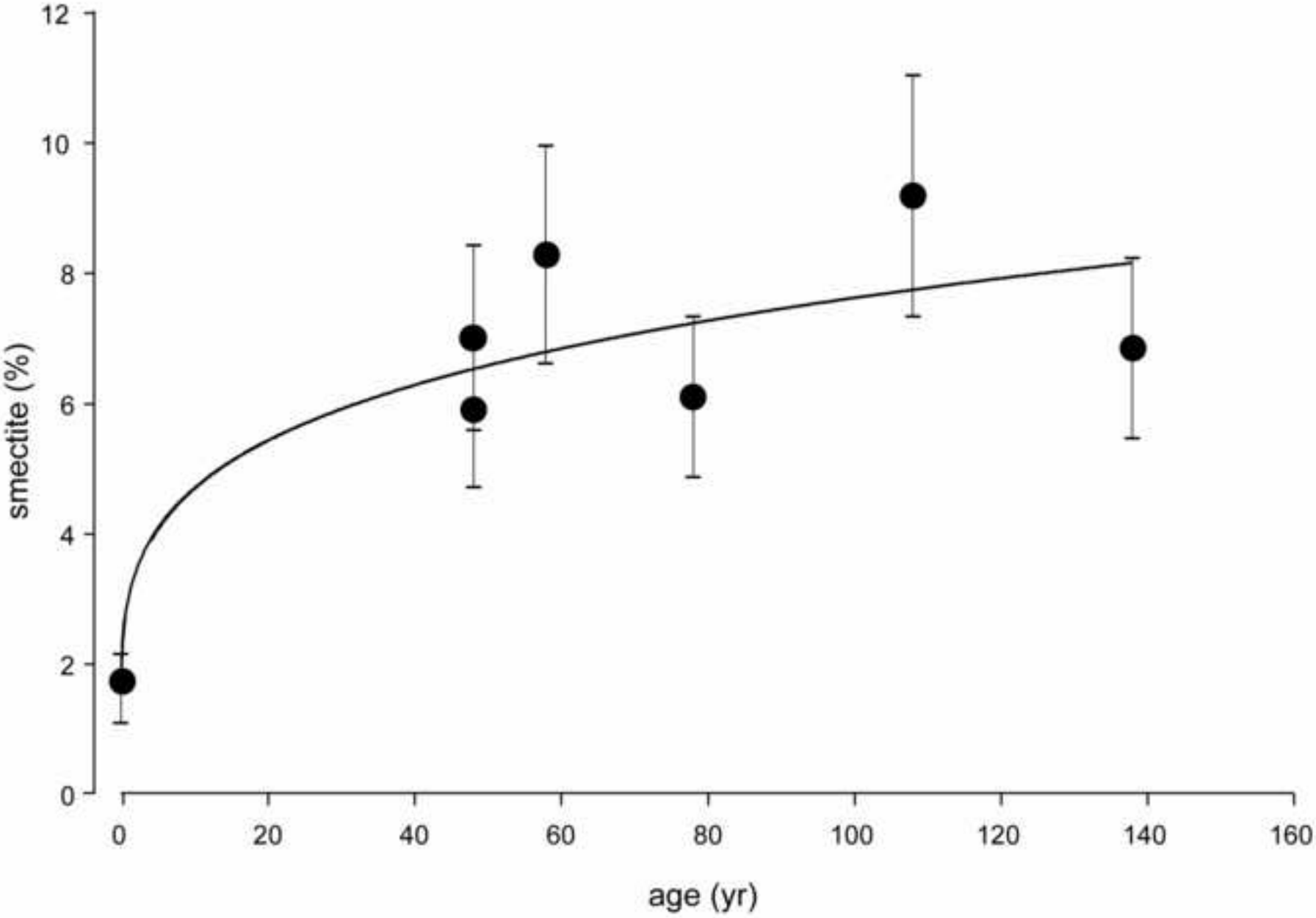

Figure 11

Click here to download high resolution image

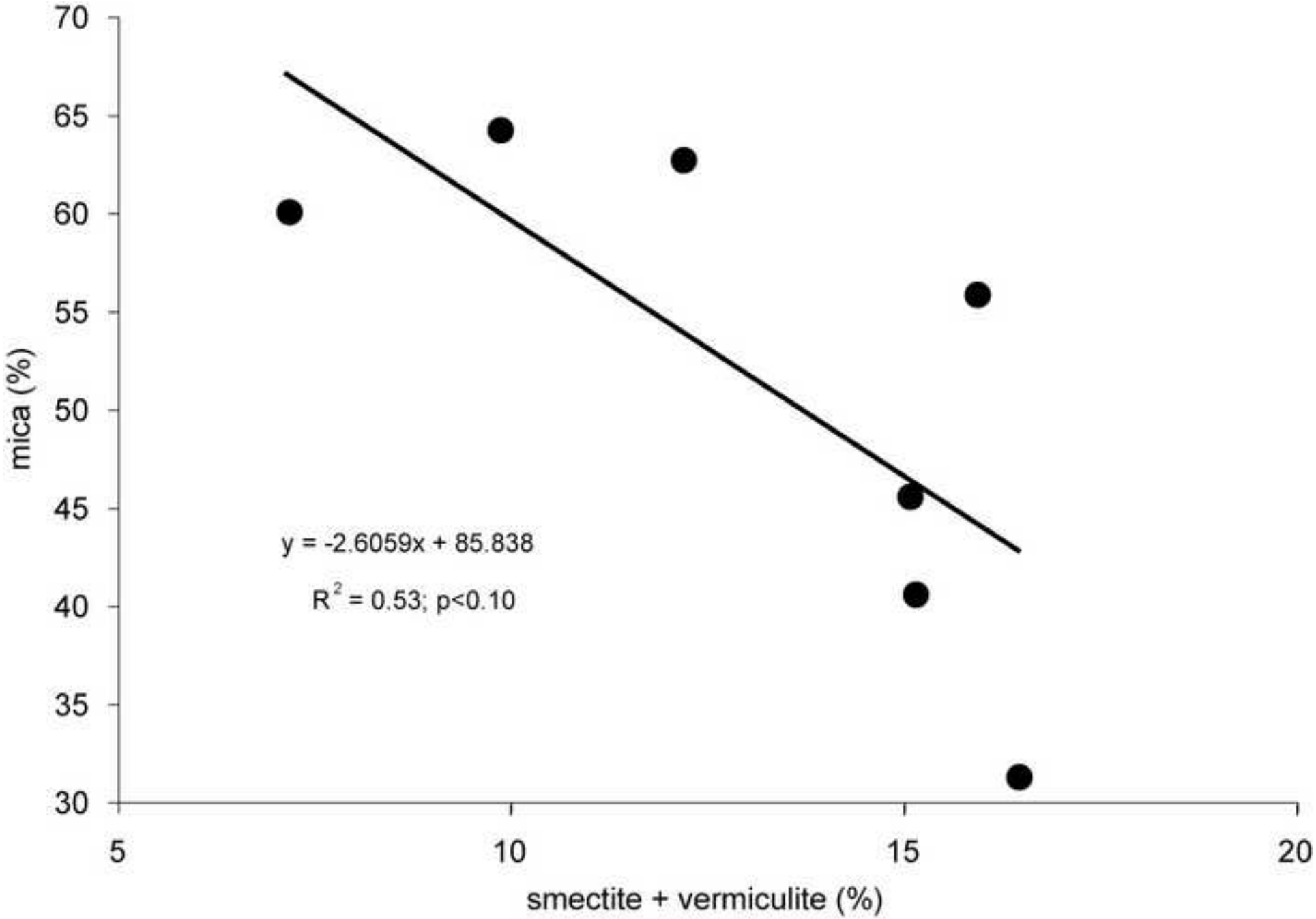

Table 1. General features of the Morteratsch proglacial area.

Latitude	46°26'N
Longitude	9°56'E
Elevation at glacier front	2117 m asl
Elevation at pro-glacial area front	1900 m asl
Main orientation	North
Geology	Granite and granodiorite (Bernina nappe, Stretta lithostratigraphic formation)
Mean annual temperature	0.5 °C
Mean annual precipitation	1100 – 1300 mm
Mean slope	<10°

Table 2. Some properties of the monitored soil sites.

Site/Soil	Soil age (yr)	Horizons	Depth (cm)	Skeleton (wt. - %)	Sand (g/kg)	Silt (g/kg)	Clay (g/kg)	pH ($CaCl_2$)
S1/Humi-Skeletic Leptosol	138	O	0-6	41	n.m.*	n.m.	n.m.	4.60
		A	6-9	50	777	184	39	4.80
		BC	9-14	53	830	158	12	4.70
		C	14-30	40	757	222	21	4.60
S2/Humi-Skeletic Leptosol	128	A	0-10	64	754	204	42	4.85
		AC	10-40	68	695	272	33	4.90
S3/Humi-Skeletic Leptosol	108	A	0-3	54	667	265	68	5.10
		AC	3-15	70	677	281	42	4.50
S4/Humi-Skeletic Leptosol	98	A	0-1	55	939	61	15	5.30
		AC	1-5	51	939	61	15	5.20
		C	5-30	70	931	57	12	5.20
S5/Humi-Skeletic Leptosol	68	A1	0-1	7	n.m.	n.m.	n.m.	4.85
		A2	1-4	1	530	432	38	4.55
		C1	4-9	36	573	387	40	4.65
		C2	9-20	64	570	372	58	4.60
S6/Skeletic Leptosol	48	A	0-2.5	64	n.m.	n.m.	n.m.	4.80
		C	2.5-25	68	852	129	19	5.00
S7/Skeletic Leptosol	48	A	0-4	26	n.m.	n.m.	n.m.	6.10
		C1	4-11	37	823	146	31	5.20
		C2	11-34	67	747	211	42	5.10

S8/Skeletic Leptosol	58	OA	0-12	63	n.m.	n.m.	n.m.	4.60
		C	12-33	48	712	220	68	4.40
S9/Humi-Skeletic Leptosol	73	O	0-3	44	n.m.	n.m.	n.m.	5.15
		AC	3-10	65	785	175	40	4.40
		C	10-36	58	832	133	35	4.65
S10/Humi-Skeletic Leptosol	78	A1	0-2	49	n.m.	n.m.	n.m.	4.70
		A2	2-10	68	818	143	39	4.50
		AC	10-25	84	733	219	48	4.80

* n.m. = not measured

Table 3
Click here to download Table: Table 3.doc

Table 3. Clay mineral content (with error range) after standard and Na-citrate treatment.

	Site	Age (yr)	Horizon	Clay phases (%)						
				Smectite	Mica	Chlorite	Vermiculite	HIV	Kaolinite	Mica/HIV
standard treatment	S1	138	A	6.9 (±1.4)	62.9 (±9.4)	2 (±0.4)	5.4 (±1.1)	0.5 (±0.3)	9.1 (±1.8)	22.1 (±3.3)
	S3	108	A	9.2 (±1.8)	31.4 (±4.7)	1.4 (±0.3)	7.3 (±1.5)	0.9 (±0.3)	4.5 (±0.9)	49.0 (±7.4)
	S6	48	A	7.0 (±1.4)	40.7 (±6.1)	2.9 (±0.6)	8.1 (±1.6)	2 (±0.4)	6.7 (±1.3)	38.1 (±5.7)
	S7	58	A	5.9 (±1.2)	64.4 (±9.7)	3.0 (±0.6)	4.0 (±0.8)	0.1 (±0.3)	6.7 (±1.3)	22.2 (±3.3)
	S8	58	OA	8.3 (±1.7)	45.7 (±6.9)	2.0 (±0.4)	6.8 (±1.4)	0.1 (±0.3)	11.8 (±2.4)	33.9 (±5.1)
	S10	78	A	6.1 (±1.2)	56.0 (±8.4)	4.1 (±0.8)	9.8 (±2.0)	0.0	6.6 (±1.3)	24.0 (±3.6)
	parent material	0	C*	1.7 (±0.4)	59.2 (±8.9)	1.8 (±0.4)	6.3 (±1.3)	0.5 (±0.1)	8.6 (±1.7)	28.6 (±4.3)
Na-citrate treatment	S1	138	A	14.7 (±2.9)	32.1 (±4.8)	4.0 (±0.8)	19.3 (±3.9)	0.9 (±0.3)	9.4 (±1.9)	19.5 (±2.9)
	S3	108	A	14.6 (±2.9)	44.9 (±6.7)	5.9 (±1.2)	7.1 (±1.4)	2.3 (±0.5)	6.8 (±1.4)	17.4 (±2.6)
	S6	48	A	15.8 (±3.2)	46.2 (±6.9)	6.3 (±1.3)	5.8 (±1.2)	3.6 (±0.7)	7.1 (±1.4)	15.2 (±2.3)
	S7	58	A	6.1 (±1.2)	66.0 (±9.9)	1.4 (±0.3)	4.1 (±0.8)	0.6 (±0.3)	9.5 (±1. 9)	10.9 (±1.6)
	S8	58	OA	11.1 (±2.2)	36.9 (±5.5)	2.2 (±0.4)	14.4 (±2.9)	3.1 (±0.6)	11.0 (±2.2)	20.5 (±3.1)
	S10	78	A1	10.7 (±2.2)	46.2 (±6.9)	2.3 (±0.5)	13.6 (±2.7)	2.2 (±0.4)	9.2 (±1.8)	16.0 (±2.4)
	parent material	0	C	3.2 (±0.6)	62.1 (±9.3)	5.0 (±1.0)	5.8 (±1.2)	2.0 (±0.4)	9.5 (±1.9)	14.9 (±2.2)

* combination of parental material from sites S1, S3, S6, S7, S8, S10 and fresh sediments from the glacier front